Chapter 3

Electrical Characterization of Mg-Doped GaN

3.1 Introduction

GaN based devices offer great potential for applications such as blue light-emitting diodes (LEDs), blue lasers, and high-power electronics. Both n- and p-type doping techniques are needed for the design of these devices. Si is generally used as a shallow n-type dopant for GaN, while shallow p-type dopants do not exist because GaN has a small permittivity of ~9. So far, Mg is the commonly used dopant which generates p-type conductivity in GaN grown by molecular beam epitaxy (MBE) and metal-organic chemical-vapor deposition (MOCVD). In addition, treatments such as electron-beam irradiation and thermal annealing are required to attain the p-type conduction in Mg-doped GaN (GaN:Mg) layers grown by MOCVD [1,2]. The electronic characteristics of Mg acceptor levels in GaN are, however, not well understood. Up to the present date, several energy levels have been detected and attributed to Mg acceptors for GaN:Mg by using various characterization techniques [3-15].

Switching gear to EV electronic applications, selective-area growth of p-type GaN and/or p-type implantation doping are required to realize power devices with a normally-off operation. From this point of view, it is very important to establish electrical characterization techniques for p-type GaN.

Tanaka *et al.* [3] reported two activation energies, 125 and 157 meV from Hall-effect measurements of samples grown by MOCVD. Johnson *et al.* [4] obtained an activation energy of 131 meV for the Mg acceptor in MOCVD-grown samples from dark current measurements. Huang *et al.* [5] measured an energy level 136 meV above the valence band in MOCVD-grown samples with a high concentration of electrically active Mg acceptors, and two energy levels 124 and 160 meV above the valence band in samples

with a lower density of electrically active Mg acceptors, using a thermal admittance spectroscopy (TAS) technique. Recently, Seghier and Gislason [6] have reported that an activation energy of 130 meV above the valence band is attributed to an Mg-related acceptor from TAS and dark current measurements.

In general, capacitance deep-level transient spectroscopy (*C*-DLTS) is the most sensitive technique to detect and characterize deep levels in the space charge region of Schottky- or pn-junction diodes on semiconductors. However, the *C*-DLTS cannot be successfully used to characterize Mg-related deep levels in GaN:Mg owing to the low diode capacitance level at low measurement temperatures [5]. In principle, the *C*-DLTS relies on a shallow background doping to ensure constant depletion width. Thus, the *C*-DLTS measurements could be conducted in a temperature range where the Mg-acceptors are fully ionized in GaN:Mg. In contrast, a current deep-level transient spectroscopy (*I*-DLTS) technique has the advantage of ability to sensitively measure deep levels in semi-insulating semiconductors in which the dopant itself is deep and/or is only partially ionized at measurement temperatures. Thus, the *I*-DLTS is better suited for the study of the Mg deep acceptor in GaN:Mg. However, this technique has a disadvantage compared to the *C*-DLTS in view of quantitative analysis. In section 3.2, we report the electrical characterization of GaN:Mg using the *I*-DLTS technique in order to detect the electronic states associated with Mg doping, comparing with the conventional TAS data.

In GaN materials and device fabrication, acceptor doping has long been a serious problem. So far, Mg is the dopant most commonly used to generate p-type conductivity in GaN, as stated above [1,2]. The acceptor levels of Mg become an important parameter in improving the performance of the doping process. Many investigations have determined that the thermal activation energy of Mg acceptors is between 120 and 250 meV by using various characterization techniques such as the Hall-effect, TAS, and *I*-DLTS measurements [3-16]. The wide range of measured data for the Mg acceptor levels may be caused by the inconsistencies in the activation conditions and/or the Mg doping concentrations in GaN:Mg. In section 3.3, we have focused on the annealing temperature used for thermal activation of the Mg dopant and systematically investigated the acceptor levels associated with Mg doping from the viewpoint of annealing

temperature by using TAS and *I*-DLTS techniques.

3.2 Current Deep-Level Transient Spectroscopy

3.2.1 Experimental

The epitaxial GaN:Mg films used in these experiments were 4 μm thick. They were grown on c-plane sapphire substrates by atmospheric pressure MOCVD at 1000 °C, with a pre-deposited 20 nm AlN buffer layer grown at 400 °C. Hydrogen was used as the main process gas and also as the carrier gas for the metal-alkyls. Trimethylgallium (TMGa), ammonia and bis-cyclopentadienyl magnesium (Cp_2Mg) were respectively used as the sources of Ga, N, and Mg. After growth, a 200-nm-thick SiO_2 layer was deposited on the top surface of the sample by radio-frequency sputtering at room temperature to provide an encapsulation cap for the subsequent activation annealing, and rapid thermal annealing (RTA) was performed at 850 °C for 20 min with halogen-tungsten lamps in flowing N_2. The heat-up time to the annealing temperature was ~10 s and temperature overshoot was minimized (< 1 °C). During the annealing, the sample was in thermal contact with a Si wafer and the temperature was measured with a calibrated thermocouple attached to the Si wafer. Following the anneal step, HF (49 % conc.) was used to remove the SiO_2 cap. Electrical measurements were conducted on the fabricated lateral dot-and-ring Schottky diodes as follows. First, ohmic contacts were made by Ni-evaporation and subsequent annealing at 500 °C for 30 min in flowing N_2. Then Pt was evaporated as Schottky contacts. The dot Pt-electrode has a diameter of 500 μm, surrounded by a ring Ni-electrode with a 1 mm gap. The area of the ring electrode was 100 times greater than that of the dot electrode. Electrical characterization of the fabricated Schottky diode has been performed by means of the self-produced equipment as shown in Fig. 3.1. Current-voltage (*I-V*) measurements were carried out at room temperature in the dark and good rectifier characteristics of the p-type Schottky diode were confirmed. The leakage current at a reverse bias of -5 V was -46.3 $\mu A/cm^2$. Frequency dependence of capacitance and capacitance-voltage (*C-V*) measurements were performed at room temperature in the dark with an ac modulation level of 15 mV and a frequency ranging from 100 Hz to 10

MHz. TAS measurements were conducted in the dark at an ac modulation level of 15 mV and a frequency ranging from 100 Hz to 30 kHz in a temperature range from 85 to 300 K. *I*-DLTS measurements were also carried out over a temperature range from 85 to 300 K. The steady state reverse bias and filling pulse voltages were -5 and 0 V, respectively. The width of the filling pulse was 1 ms, which ensured that even traps with very small hole capture cross-sections were completely saturated.

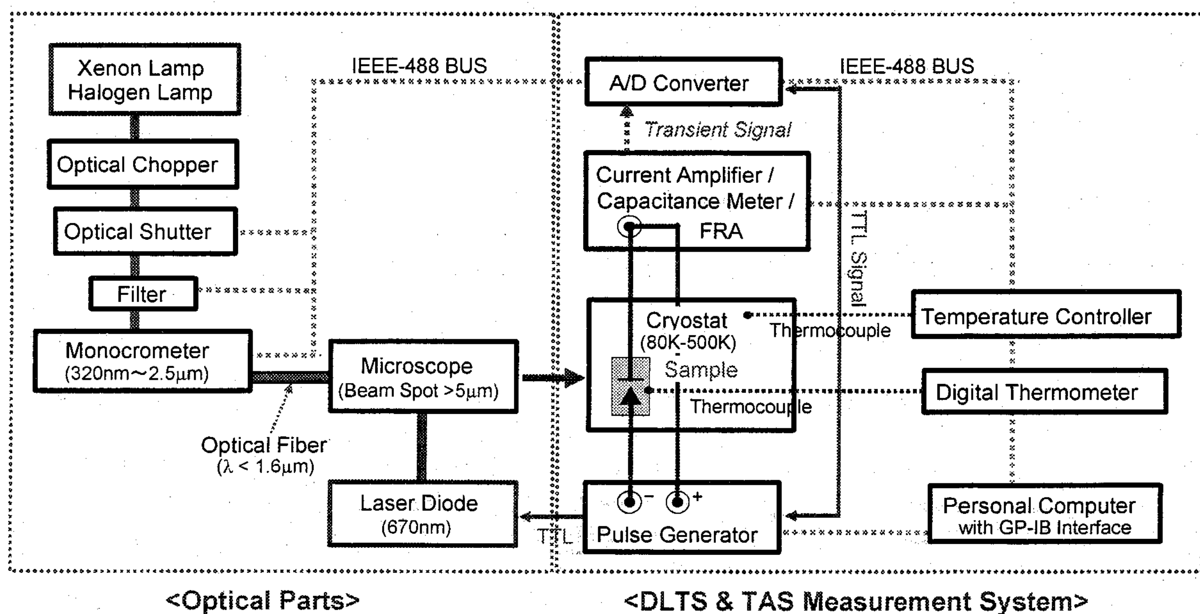

FIG. 3.1. A schematic of self-produced electrical characterization system equipped with optical parts.

3.2.2 Results and Discussion

Figure 3.2 shows room-temperature frequency dependence of capacitance at a zero dc bias and $1/C^2$-V plots for the fabricated Pt-Schottky diode. The capacitance is seen to be strongly frequency dependent. The capacitance is reduced at frequencies higher than 30 kHz. This variation in capacitance is most likely due to a typical dispersion effect, which occurs when a deep level is unable to follow the high-frequency voltage modulation and contributes to the net space charge in the depletion region. Here, the Mg level acts

simultaneously as a deep impurity and a dopant. Depending on frequency, there is a competition between the deep impurity and the dopant character. In the low frequency range, the holes provided by the modulating voltage essentially modify the charge on the impurity level. Thus, the low frequency capacitance remains nearly constant in this range. When these holes are no longer able to follow the applied voltage modulation, the holes contribute to the modulation of the depletion layer charge, but with a stronger amplitude than in the low frequency range. In other words, the low frequency capacitance is determined by the carrier exchange between the Mg-related impurity level and the valence band, whereas above the impurity transition frequency, the hole modulation of the depletion layer edge governs the electrical response. Considering the frequency dependence of capacitance as shown in the inset of Fig. 3.2, meaningful *C-V* measurements need to be performed at lower frequencies. It is also found that the conventional *C*-DLTS measurements using a high-frequency type capacitance meter could not be successfully used to characterize the Mg-related levels as stated above, because the capacitance measurement is unreliable at frequencies

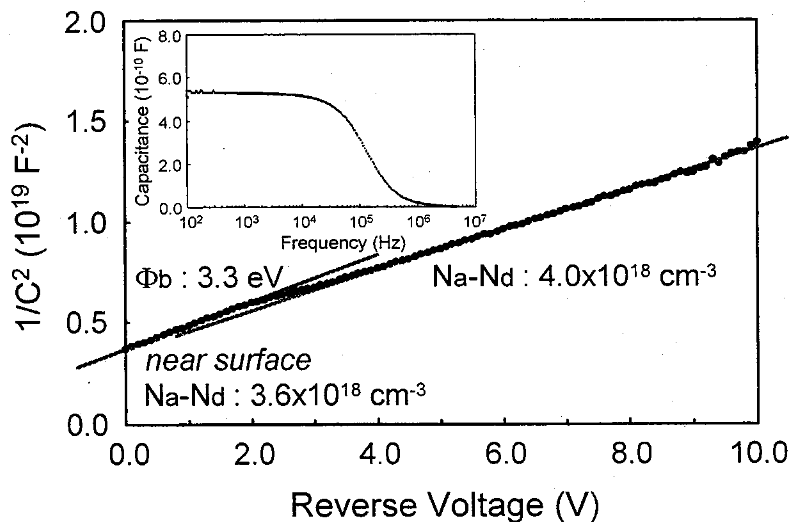

FIG 3.2. Room-temperature capacitance-voltage characteristics at a frequency of 1 kHz. The inset shows frequency dependence of capacitance at room temperature.

above 30 kHz. Instead, TAS and I-DLTS techniques are more suitable for the electrical characterization of the Mg acceptor levels. As shown in Fig. 3.2, $1/C^2$-V plots at the low frequency of 1 kHz reveal that an effective acceptor concentration (N_a - N_d) of ~4x10^{18} cm^{-3} almost uniformly distributes over the depth of the capacitance measurement. This value is in good agreement with the Mg concentration determined by secondary ion mass spectrometry (SIMS). In the case of acceptors in GaN:Mg, the C-V measurements at 1 kHz determine the net acceptor concentration (minus the concentration of donors) rather than the hole concentration. Strictly speaking, in the near surface region of ~40 nm, the acceptor concentration is slightly reduced, which indicates that the dissociation of GaN in the near surface region is induced by the activation annealing process. By extrapolating the line fitted to the $1/C^2$-V plots to the voltage axis as shown in Fig. 3.2, the barrier height ϕ_b of the fabricated Pt-Schottky diode is estimated to be ~3.3 eV.

Figure 3.3 shows TAS spectra measured on the fabricated Pt-Schottky diode sample at various frequencies under a zero dc bias. A peak can be clearly seen in the spectra. This peak shifts to higher temperatures with increasing measurement frequency. Thus, this peak is related to a deep level. Arrhenius analysis for hole emission rate e_p/T^2 of the corresponding level yields an activation energy of ~115 meV for hole emission into the valence band. Here, the data was analyzed under the assumption of a temperature-independent cross-section.

Figure 3.4 shows I-DLTS spectra measured on the Pt-Schottky diode sample at various rate-windows. A dominant peak can be clearly detected in the spectra. This peak shifts to higher temperatures with increasing the hole emission rate calculated from the rate-windows, which indicates that this peak is assigned to a hole trap. As shown in Fig. 3.5, an activation energy from the top of the valence band is calculated to be ~112 meV from the slope of the line fitted to the Arrhenius plots of hole emission rate e_p/T^2 for this peak. This value is very close to an activation energy of ~115 meV for the TAS measurements, indicating that both energy levels detected by TAS and I-DLTS measurements are attributed to an identical deep level. Here, the characteristic frequency associated with this energy level at room temperature (295 K) is estimated to be

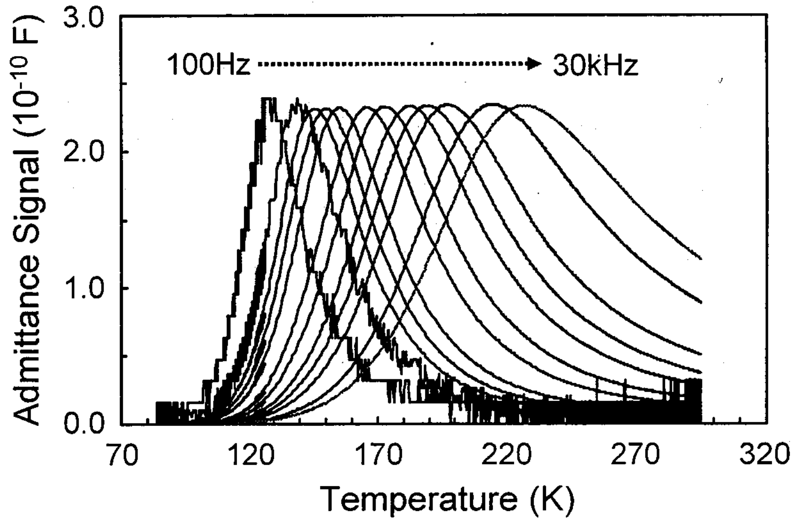

FIG. 3.3. TAS spectra at various frequencies of 100 Hz - 30 kHz for the Mg-doped GaN.

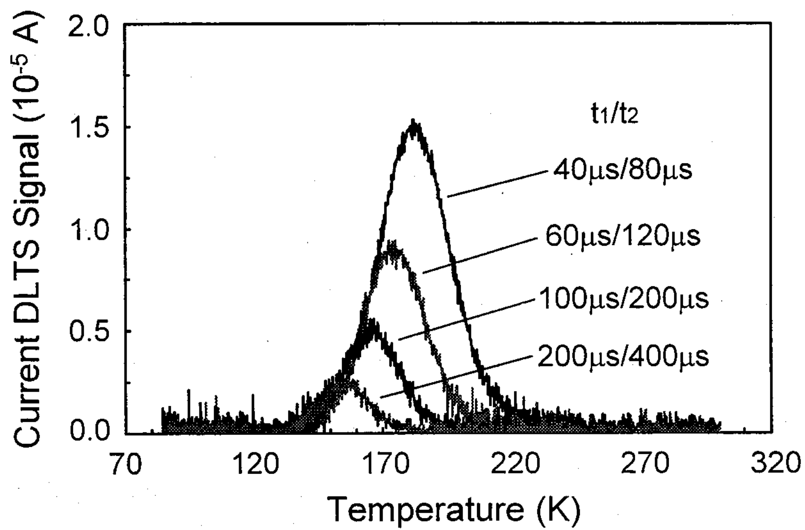

FIG. 3.4. Current DLTS spectra at various rate-windows for the Mg-doped GaN.

~95.9 kHz, extracting from the line fitted to the Arrhenius plots as shown in Fig. 3.5 [5]. This frequency is found to be in reasonable agreement with one estimated from the frequency dependence of capacitance at room temperature as shown in the inset of Fig. 3.2. Therefore, this energy level revealed by TAS and *I*-DLTS for our sample is considered to be assigned to the Mg deep acceptor itself, possessing an activation energy which is apparently lower than the results previously reported in the literature [3-6]. Additionally, no other centers deeper than this Mg acceptor show up in the TAS and *I*-DLTS spectra for our sample.

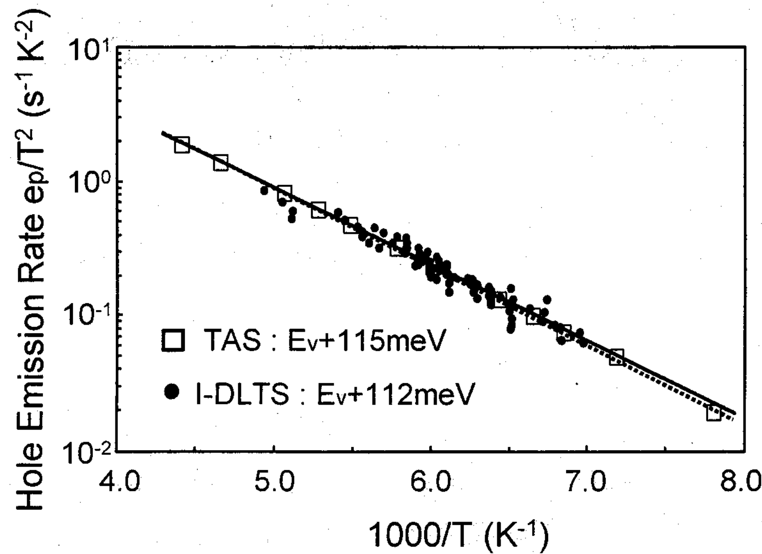

FIG. 3.5. Arrhenius plots of hole emission rate e_p/T^2 for the Mg-doped GaN.

For reference, we also prepared an activation annealed sample with the same Mg-doping concentration and without a SiO_2 encapsulation cap to confirm whether this lower activation energy for the Mg acceptor is due to the annealing conditions. A discrete energy level with a much lower activation energy of 97 meV was detected by TAS measurements for this sample. Therefore, this lowering of the activation energy for the Mg acceptor which was revealed by the TAS and *I*-DLTS measurements, is considered to be due to the presence of point defects generated in the activation annealing process, rather than the energy level splitting

observed for highly Mg-doped samples. That is, it may be attributed to the Pool-Frenkel-effect in depletion region, which is induced by applying biased voltage in the TAS and *I*-DLTS measurements.

In summary, we have investigated the GaN:Mg sample grown by MOCVD using TAS and *I*-DLTS techniques. Both measurements revealed an activation energy of ~112 meV from the valence band, which is in reasonable agreement with the frequency dependence of capacitance in view of the characteristic frequency at room temperature. Therefore, this energy level is most probably associated with the Mg acceptor state itself.

3.3 Activation Annealing Behavior of Mg Acceptors

3.3.1 Experimental

The epitaxial GaN:Mg films used in these experiments were 1.6 μm thick. They were grown on c-plane sapphire substrates by atmospheric pressure MOCVD at 1025 °C, with a pre-deposited 20 nm AlN buffer layer grown at 400 °C. Hydrogen was used both as a main process gas and as a carrier gas for metal alkyls. TMGa, ammonia, and Cp_2Mg were respectively used as the sources of Ga, N, and Mg. The Mg concentration of the as-grown GaN:Mg layer was determined to be ~4.7×10^{18} cm^{-3} by SIMS measurements. After growth, activation annealing was systematically performed at temperatures between 600 and 850 °C for 10 min in flowing N_2. The annealing temperatures for typical samples 1 - 6 are summarized in Table 3.1, together with their electrical data. Electrical characterization of acceptor levels in GaN:Mg was conducted on lateral dot-and-ring Schottky diodes fabricated as follows. First ohmic contacts were made by Ni evaporation and subsequent annealing at 500 °C for 30 min in flowing N_2. Then Pt was evaporated to form Schottky contacts. The dot Pt-electrode has a diameter of 500 μm, surrounded by a ring Ni-electrode with a 1 mm gap. The area of the ring electrode was 100 times greater than that of the dot electrode. From room-temperature *I-V* measurements in the dark, good rectifier characteristics of the p-type Schottky diode were confirmed under all the annealing conditions. Capacitance-frequency (*C-f*), conductance-frequency (*G/ω-f*), and capacitance-voltage (*C-V*) measurements were performed at room temperature in the dark with

an ac modulation level of 30 mV and frequencies ranging from 100 Hz to 10 MHz. TAS measurements were conducted in the dark at an ac modulation level of 30 mV and frequencies ranging from 100 Hz to 30 kHz in a temperature range from 85 to 320 K. *I*-DLTS measurements were also carried out over a temperature range from 85 to 320 K. The steady state reverse bias and filling pulse voltages were -3 and 1 V, respectively. The width of the filling pulse was 1 ms, which ensured that even traps with very small hole capture cross-sections were completely saturated.

TABLE 3.1. Annealing-temperature dependence of acceptor concentration studied by the room-temperature *C-V* measurements for the GaN:Mg samples.

Sample	Annealing temperature (°C)	Acceptor concentration N_a-N_d (10^{18} cm^{-3})
1	600	0.2
2	650	2.8
3	700	4.0
4	750	2.6
5	800	2.2
6	850	13.9

3.3.2 Results and Discussion

Figure 3.6 (a) shows room-temperature *C-f* curves at a zero dc bias for the Schottky diodes based on the GaN:Mg samples (samples 1 - 6) annealed at various temperatures. A typical dispersion effect characteristic of deep Mg acceptors is observed under all the annealing conditions [5]. Depending on frequency, there is a competition between the deep impurity and the dopant character. Here, the low frequency capacitance C_L is determined by the carrier exchange between the Mg-related impurity level and the valence band, reflecting the electrical activity of Mg dopant, whereas above the capacitance cutoff frequency f_c (impurity transition frequency), the hole modulation of the depletion layer edge governs the electrical response. Sample 1

shows a small f_c of ~1.9 kHz and a small C_L of ~0.35 nF, which indicates that the 600 °C annealing slightly activates the Mg dopant. In sharp contrast, a significant increase in f_c is seen in addition to a large increase in C_L for samples 2 and 3. This result suggests that the electrical activity of Mg is significantly improved by the annealing at 650 and 700 °C. More importantly, interesting behavior is observed in the high frequency region of the *C-f* and *G/ω-f* curves for these samples. Considering that the conductance *G/ω* presents a peak at the f_c, higher-frequency component peaks can be seen as shoulders at ~331.6 and ~400.7 kHz apart from the main peaks at around 30 kHz in the *G/ω-f* curves for the samples annealed at 650 and 700 °C,

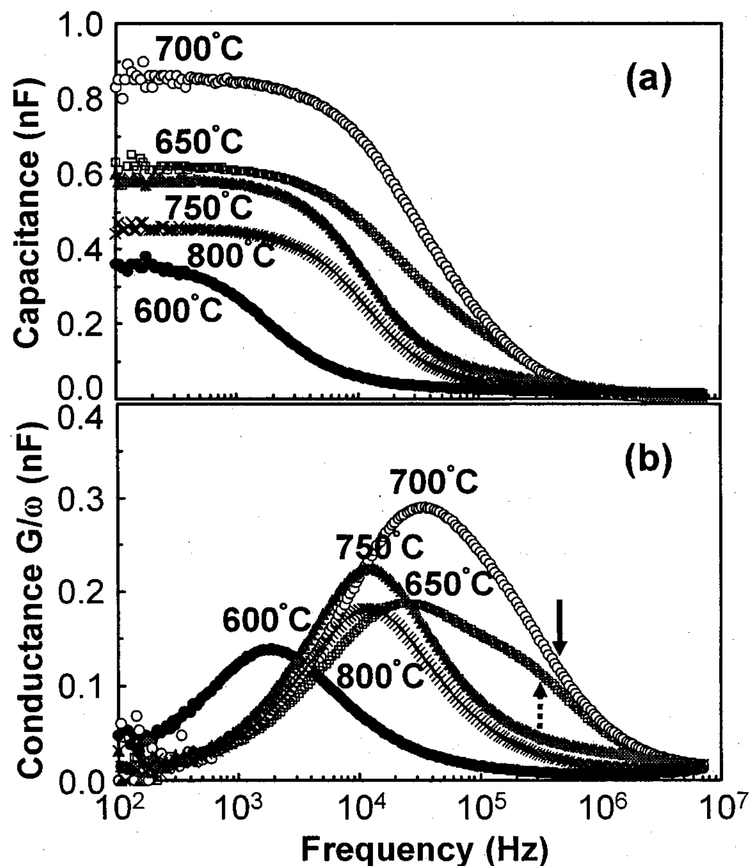

FIG. 3.6. Room-temperature frequency dependence of (a) capacitance and (b) conductance *G/ω* for the fabricated Schottky diodes based on the GaN:Mg samples annealed at various temperatures.

respectively, as shown in Fig. 3.6 (b). This indicates that shallower acceptor levels may be newly formed by the annealing at these temperatures. Furthermore, decreases in f_c and C_L are seen in accordance with the disappearance of the higher-frequency component peaks for the samples annealed at 750 and 800 °C (samples 4 and 5).

From the *C-f* data, meaningful *C-V* measurements need to be performed at lower frequencies. Thus, effective acceptor concentrations were estimated from $1/C^2$-V plots at 1 kHz, as shown in Table 3.1. Here, the obtained values imply the net acceptor concentration (N_a - N_d) rather than the hole concentration. The annealing-temperature dependence of the acceptor concentration is in good agreement with the variation in C_L of the *C-f* curves, as stated above. In particular, the acceptor concentration of sample 3 is in reasonable accord with the Mg concentration determined by the SIMS measurements, indicating that the activation annealing at around 700 °C significantly enhances electrical activation rate of Mg dopant. Furthermore, the acceptor concentration uniformly distributes over the depth of the capacitance measurements for the samples annealed at temperatures below 800 °C (samples 1 - 5), whereas the concentration becomes very high for the sample annealed at 850 °C (sample 6). From the SIMS measurements, Mg is found to diffuse out towards the near-surface region of ~200 nm from the surface by the 850 °C annealing, as shown in Fig. 3.7. This segregation phenomenon of the Mg dopant starts to occur by the annealing at around 800 °C.

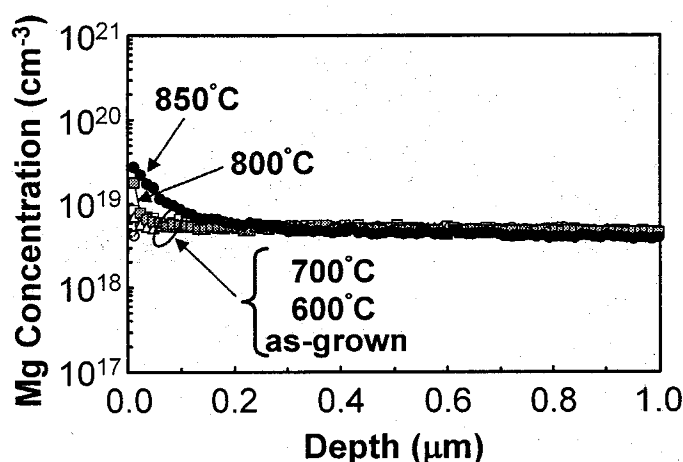

FIG. 3.7. SIMS profiles of Mg in GaN:Mg samples, as-grown and annealed at various temperatures.

Figures 3.8 and 3.9 respectively show a typical series of TAS and *I*-DLTS spectra for the Schottky diodes based on the GaN:Mg samples (samples 1 - 6) annealed at various temperatures. Both spectra yield identical information about deep acceptor levels in GaN:Mg. Depending on annealing temperature, both spectra reveal three kinds of peaks which are denoted A_0, A_1, and A_2. These peaks shift towards higher temperatures with increasing hole emission rate which can be calculated from the measurement frequency and the rate window t_1/t_2 for TAS and *I*-DLTS measurements, respectively. This implies that these peaks are assigned to deep acceptor levels associated with the Mg dopant. From Arrhenius plots of hole emission rate e_p/T^2 of the corresponding level in the both spectra as shown in Fig.3.10, thermal activation energies for hole emission into the valence band were estimated. Here, the data were analyzed under the assumption of a temperature-independent cross-section. The data obtained from the TAS measurements were very close to those for the *I*-DLTS measurements. For the sample annealed at 600 °C (sample 1), a weak broad peak A_0 is detected, corresponding to a deep acceptor level of Mg with the thermal activation energy of ~161 meV above the valence band. This acceptor level has much smaller cross-section than the other acceptor levels (A_1 and A_2), which indicates that the A_0 level is probably in the early stage of the Mg acceptor formation, resulting in the slightly electrical activation of the Mg dopant as stated above. For the samples annealed at 650 and 700 °C (samples 2 and 3), two peaks A_1 and A_2 which are clearly different from the first peak A_0, are observed. The thermal activation energies for the acceptor levels A_1 and A_2 are ~160 and ~135 meV from the valence band, respectively. These values are consistent with the reported values in the literature [5,6,13]. Moreover, the A_2 peak is seen to disappear in the both spectra by the 750 °C annealing (sample 4). By combining these results with the *C-f*, *G/ω-f*, and *C-V* data, the presence of the A_2 level seems to be related to the large increases in f_c and effective acceptor concentration, as stated above. In particular, the A_2 level probably corresponds to the higher-frequency component peaks observed in the *G/ω-f* curves for the samples annealed at 650 and 700 °C (samples 2 and 3). Thus, the shallower A_2 level is most likely to dominantly improve the electrical Mg activity in GaN:Mg [6]. Furthermore, the thermal activation energy of the A_1 level is found to decrease from ~160 to ~145 meV with increasing annealing temperature from 750 up to 850

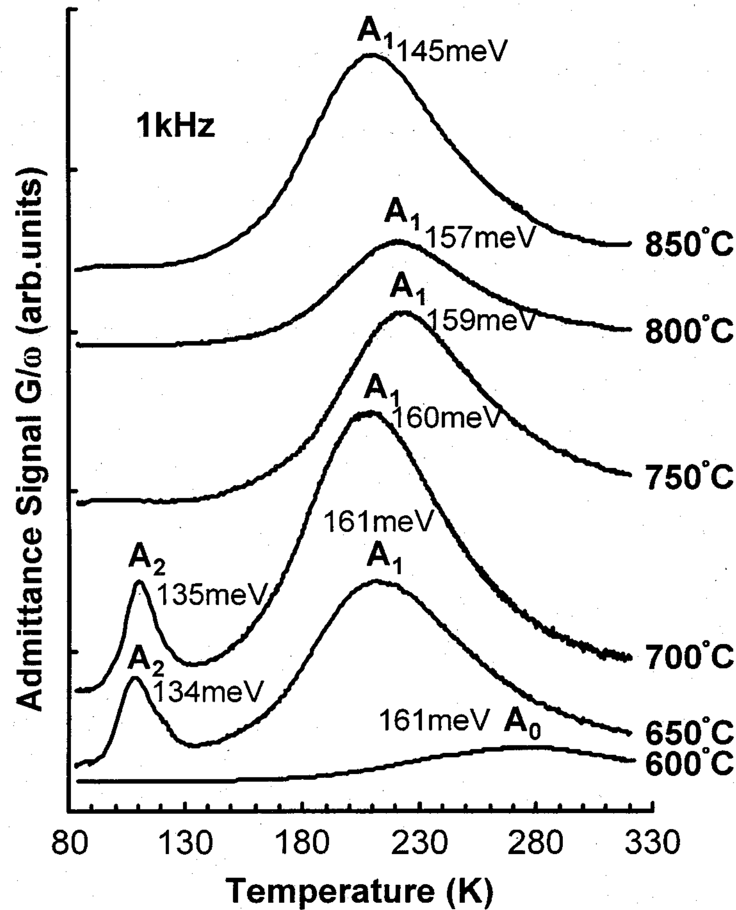

FIG. 3.8. TAS spectra at the frequency of 1 kHz for the fabricated Schottky diodes based on the GaN:Mg samples annealed at various temperatures.

°C (samples 4, 5, and 6) in both the TAS and *I*-DLTS measurements. This lowering of the activation energy for the A_1 level may be related to the Mg motion induced by the high-temperature annealing process. Additionally, the *I*-DLTS spectrum shows a large increase in concentration of the A_1 level for the sample annealed at 850 °C (sample 6), which is in good agreement with the segregation phenomenon of the Mg dopant as confirmed by the SIMS measurements. Therefore, the continued reconfiguration of the local

region surrounding Mg atoms may induce the energy level splitting of the A_1 level, resulting in the lowering of the activation energy [18]. The activation energies observed should be also subject to the Poole-Frenkel field effect which is apt to occur in the TAS and *I*-DLTS measurement techniques [9,17].

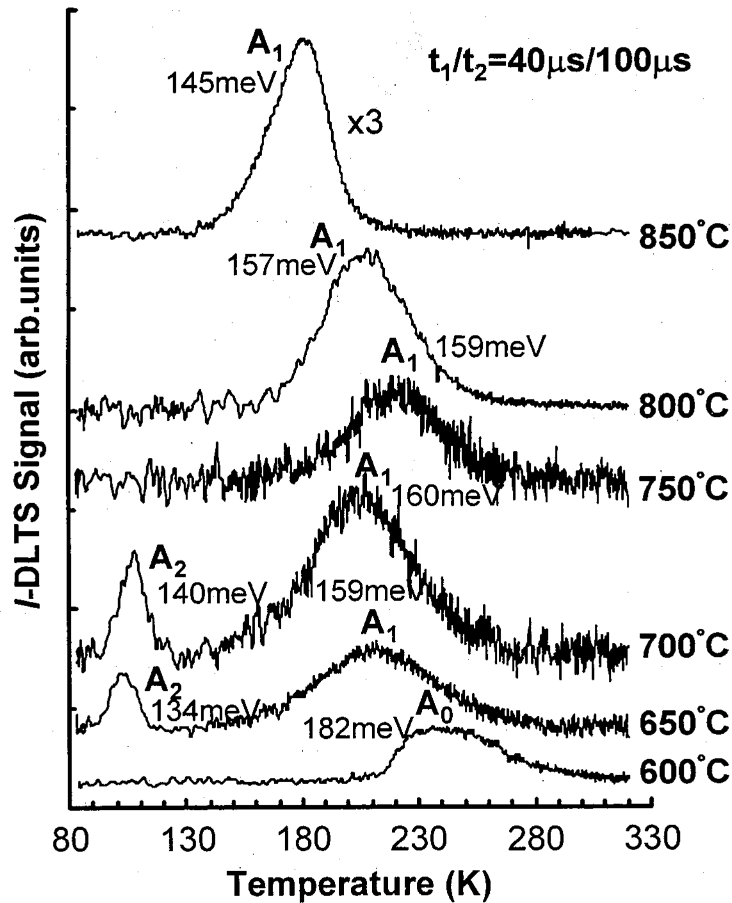

FIG. 3.9. *I*-DLTS spectra at the rate windows t_1/t_2 of 40 μs/100 μs for the fabricated Schottky diodes based on the GaN:Mg samples annealed at various temperatures.

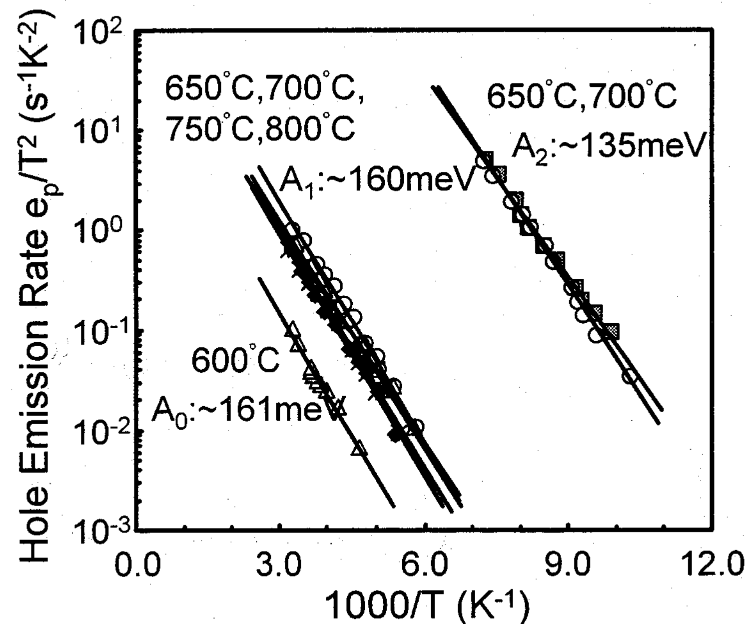

FIG. 3.10. Arrhenius plots of hole emission rate e_p/T^2 for the GaN:Mg samples annealed at various temperatures.

In summary, we have systematically investigated the annealing-temperature dependence of acceptor levels in GaN:Mg samples grown by MOCVD by using TAS and *I*-DLTS techniques. Both measurements reveal two deep acceptor levels with thermal activation energies of ~135 and ~160 meV from the valence band. The annealing behavior of the former level is in reasonable agreement with the variation in the effective acceptor concentration. Therefore, this acceptor level is considered to dominate the electrical activity of Mg in GaN.

3.4 Conclusion

The *I*-DLTS measurement technique as well as the TAS one was found to be effective in electrical characterization of deep acceptor levels in Mg-doped GaN. These *I*-DLTS and TAS techniques have been applied on Schottky diodes based on Mg-doped GaN grown by MOCVD to investigate dependence of Mg

acceptor levels on annealing temperature. Both measurements revealed two deep acceptor levels with activation energies of ~135 and ~160 meV above the valence band. The former level is seen only when the samples were annealed at temperatures between 650 and 700 °C, and its presence is in reasonable agreement with a significant increase in effective acceptor concentration confirmed by low-frequency *C-V* measurements. Therefore, this acceptor level is considered to dominate the electrical activation of Mg in GaN.

References

[1] H. Amano, M. Kito, K. Hiramatsu, and I. Akasaki, Jpn. J. Appl. Phys. **28**, L2112 (1989).

[2] S. Nakamura, T. Mukai, M. Senoh, and N. Iwasa, Jpn. J. Appl. Phys. **31**, L139 (1992).

[3] T. Tanaka, A. Watanabe, H. Amano, Y. Kobayashi, K. I. Akasaki, S. Yamazaki, and M. Koide, Appl. Phys. Lett. **65**, 593 (1994).

[4] C. Johnson, J. Y. Lin, H.X. Jiang, M. A. Khan, and C. J. Sun, Appl. Phys. Lett. **68**, 667 (1996).

[5] J. W. Huang, T. F. Kuech, H. Lu, and I. Bhat, Appl. Phys. Lett. **68**, 2392 (1996).

[6] D. Seghier and H. P. Gislason, Appl. Phys. Lett. **88**, 6483 (2000).

[7] W. Götz, N. M. Johnson, J. Walker, D.P. Bour, and R.A. Street, Appl. Phys. Lett. **68**, 667 (1996).

[8] J. Z. Li, J. Y. Lin, H. X. Jiang, A. Salvador, A. Botchkarev, and H. Morkoc, Appl. Phys. Lett. **69**, 1474 (1996).

[9] D. J. Kim, D. Y. Ryu, N. A. Bojarczuk, J. Karasinski, S. Guha, S. H. Lee, and J. H. Lee, J. Appl. Phys. **88**, 2564 (2000).

[10] M. Schmeits, N. D. Nguyen, and M. Germain, J. Appl. Phys. **89**, 1890 (2001).

[11] A. Y. Polyakov, N. B. Smirnov, A. V. Govorkov, A. S. Usikov, N. M. Shmidt, and W. V. Lundin, Solid-State Electronics **45**, 255 (2001).

[12] W. Götz, N. M. Johnson, and D. P. Bour, Appl. Phys. Lett. **68**, 3470 (1996).

[13] R. Y. Korotkov, J. M. Gregie, and B. W. Wessels, Appl. Phys. Lett. **78**, 222 (2001).

[14] E. Litwin-Staszewska, T. Suski, R. Piotrzkowski, I. Grzegory, M. Bockowski, J. L. Robert, L. Kończewicz, D. Wasik, E. Kamińska, D. Cote, and B. Clerjaud, J. Appl. Phys. **89**, 7960 (2001).

[15] N. D. Nguyen, M. Germain, M. Schmeits, B. Schineller, and M. Heuken, J. Appl. Phys. **90**, 985 (2001).

[16] Y. Nakano and T. Kachi, Appl. Phys. Lett. **79**, 1631 (2001).

[17] D. J. Kim, J. Appl. Phys. **88**, 1929 (2000).

[18] Y. Nakano and T. Jimbo, J. Appl. Phys. **92**, 5587 (2002).

[19] Y. Nakano, R. K. Malhan, T. Kachi, and H. Tadano, J. Appl. Phys. **89**, 5961 (2001).

Chapter 4

P-Type Implant Doping of GaN

4.1 Introduction

GaN is of increasing interest for high-temperature and high-power electronic devices [1-3]. In order to facilitate the design of these electronic devices, especially from a selective-area doping point of view, both n- and p-type implantation-doping technologies are considered as being essential. Si is generally used as a shallow n-type dopant for GaN, while shallow p-type dopants do not exist because GaN has a relatively small permittivity of ~9. Thus, acceptor doping has long been a serious problem for both GaN materials and device fabrication. The most commonly used p-type dopant is Mg, which has an ionization energy of 150 - 200 meV above the valence band [4-7]. In the case of Mg implantation doping, however, it is very difficult to achieve p-type conductivity at room temperature, because implantation-induced damage may easily compensate the holes generated from Mg acceptors due to its heavy ion mass in addition to their deep acceptor levels [8,9]. On the other hand, Be is expected theoretically to be a more promising candidate for p-type doping since its ionization energy is calculated to be ~60 meV when residing on Ga-lattice sites in Wurtzite GaN [10,11]. Additionally, the light Be atoms can be implanted deeper into GaN for a given implantation energy, and they cause less damage in the GaN lattice than Mg atoms.

So far, Be-doped GaN (GaN:Be) films have only been grown by molecular beam epitaxy (MBE) [12,13]. Recently, some data on Be acceptors have been reported; Salvador *et al.* [13] have obtained an ionization energy of about 250 meV from photoluminescence (PL) measurements of GaN:Be samples grown by MBE. Ronning *et al.* [14] have reported that isolated Be has the most shallow acceptor level, with an ionization energy of 150 ± 10 meV from PL measurements of Be-implanted GaN samples. Clearly the literature does

not provide a coherent value for these acceptor levels. In addition, no electrical characterization of the acceptor levels associated with Be doping has been reported as yet, and the acceptor levels are an important parameter in improving the performance of the p-type doping process. Thus, various investigations need to be performed to determine the Be acceptor levels by using electrical and optical characterization techniques. In this chapter, we have focused on the electrical characterization of Be-implanted GaN by using a thermal admittance spectroscopy (TAS) technique in order to detect the electronic states associated with Be doping.

In section 4.2, we have reported that some slight electrical p-type activity was achieved for Be-implanted GaN and that the Be-related acceptor level was located at ~231 meV above the valence band from TAS measurements [15]. This value is much deeper than the theoretically expected value. This deepening of the activation energy for Be acceptors is considered to be associated with imperfect incorporation of the implanted Be ions. In the case of conventional Be implantation, where one kind of dopant is used, the generation of many N vacancies may occur in the implanted region after the activation annealing process, resulting in Be atoms residing in interstitial sites in GaN. Therefore, in order to suppress the N vacancies, an N-rich condition should be created prior to Be implantation [8,16,17]. Considering that O atoms are apt to substitute at N-lattice sites, the implantation of additional O atoms into GaN might be expected to increase the probability that Be atoms will occupy a Ga-lattice site. In section 4.3, the acceptor levels in Be+O co-implanted GaN have been investigated electrically, and the results are compared to those of conventional Be-implanted GaN [18].

4.2 Be Implantation

4.2.1 Experimental

The epitaxial GaN films used in these experiments were 1 μm thick. They were grown on a-plane sapphire substrates by atmospheric pressure metal-organic chemical-vapor deposition (MOCVD) at 1050 °C, with a pre-deposited 20 nm AlN buffer layer grown at 400 °C. The GaN films were not intentionally doped, with a background n-type carrier concentration of ~$5x10^{15}$ cm^{-3}. Prior to the Be implantation, a

300-nm-thick SiO_2 layer was deposited on the top surface of the samples by radio-frequency (RF) sputtering in order to reduce the implantation-induced damage. Then, multiple step Be implantation was performed using pure Be metal as the source of the $^9Be^+$ species. The $^9Be^+$ ions were implanted at 150, 100, and 80 keV with dosages of $2.3x10^{14}$, $6x10^{13}$, and $6x10^{13}$ cm^{-2}, respectively, to produce a mean Be concentration of $1x10^{19}$ cm^{-3} to a depth of ~0.3 μm. For reference, N-implanted and Be+N co-implanted GaN samples was also prepared. The N-implanted sample had a mean N concentration of $1x10^{19}$ cm^{-3} (depth = 0.3 μm). The Be+N co-implanted samples enabled the N/Be ratio to change 0, 0.5, 1.0, and 2.0, respectively, with a fixed Be concentration of $1x10^{19}$ cm^{-3} (depth = 0.3 μm). All of the implants were carried out at room temperature, with an incident angle 7° off the surface normal. After implantation, the SiO_2 layer was removed and then a 500-nm-thick SiO_2 capping layer was again deposited on the top surface of the implanted samples by RF sputtering at room temperature to provide an encapsulation cap for the subsequent implant activation annealing. All of the samples were annealed in a SiC-coated graphite susceptor at 1050 °C for 5 min in flowing H_2 gas at a pressure of 10 Torr. Following the annealing step, HF was used to remove the SiO_2 cap. The depth distribution of the implanted Be atoms was measured by secondary ion mass spectrometry (SIMS). The carrier type of the Be-implanted samples could not be determined by room-temperature Hall-effect measurements because of poor data caused by extremely small Hall-voltages, as is the case for p-type GaN in general. Instead, electrical measurements were conducted on lateral dot-and-ring Schottky diodes fabricated as follows. First, ohmic contacts were deposited by Ni evaporation and subsequent annealing at 500 °C for 30 min in flowing N_2. Then Pt was evaporated to form the Schottky contacts. The dot Pt-electrode had a diameter of 500 μm, and was surrounded by a ring Ni-electrode with a 1 mm gap. The area of the ring electrode was 100 times greater than that of the dot electrode. From current-voltage (*I-V*) measurements at room temperature in the dark, the Be-implanted sample showed the rectifying characteristics of a p-type Schottky diode, while the N-implanted sample displayed the characteristics of an n-type Schottky diode in the same way as the as-grown GaN before implantation. Capacitance-frequency (*C-f*), conductance-frequency (*G/ω-f*), and capacitance-voltage (*C-V*) measurements

were performed at room temperature in the dark with an ac modulation level of 30 mV and frequencies ranging from 100 Hz to 10 MHz. TAS measurements were conducted in the dark at an ac modulation level of 30 mV and frequencies ranging from 100 Hz to 30 kHz, covering the temperature range from 85 to 475 K.

4.2.2 Results and Discussion

Figure 4.1 shows SIMS profiles of the implanted Be atoms both before and after annealing at 1050 °C, together with Be atomic profiles calculated by the Transport of Ions in Matter software (TRIM). There is little Be redistribution caused by the implant activation annealing, indicating the thermal stability of the implanted Be atoms in GaN. From this result, it is expected that diffusion of Be atoms into GaN from an external source is not practical and that ion implantation will be required if we wish to introduce Be atoms into GaN with a view to selective-area doping. The mean Be concentration to a depth of ~0.3 μm is about $1x10^{19}$ cm^{-3}, a value that is in reasonable agreement with that of the TRIM calculation. The tails

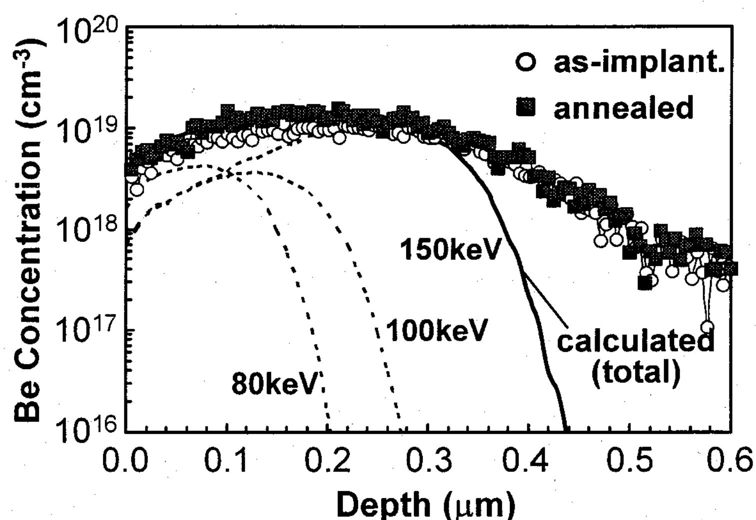

FIG 4.1. TRIM simulated atomic profiles of implanted Be (solid line) and SIMS profiles of Be implanted in GaN, as implanted (○) and annealed (■) at 1050 °C.

apparent on the bulk side of the experimental Be profiles may be caused by the high background due to the high resistivity of the Be-implanted samples.

Figure 4.2 shows room temperature C-f and G/ω-f curves at zero dc bias for a Schottky diode based on the Be-implanted GaN after annealing at 1050 °C. The capacitance is seen to be strongly frequency-dependent, as shown by the C-f curve. The capacitance is reduced at frequencies higher than 1 kHz. This variation in capacitance is most likely to be due to a typical dispersion effect that occurs when a deep level is unable to follow the high-frequency voltage modulation and contributes to the net space charge in the depletion region [6,7]. In addition, the N-implanted GaN sample showed frequency-independence of capacitance and maintained low values. These results indicate that the deep level observed in the Be-implanted sample may be associated with Be doping. That is, the Be-related level could act simultaneously as a deep impurity and as a dopant. Depending on frequency, there is a competition between the deep impurity and the dopant character. The low frequency capacitance C_L of ~50 pF is

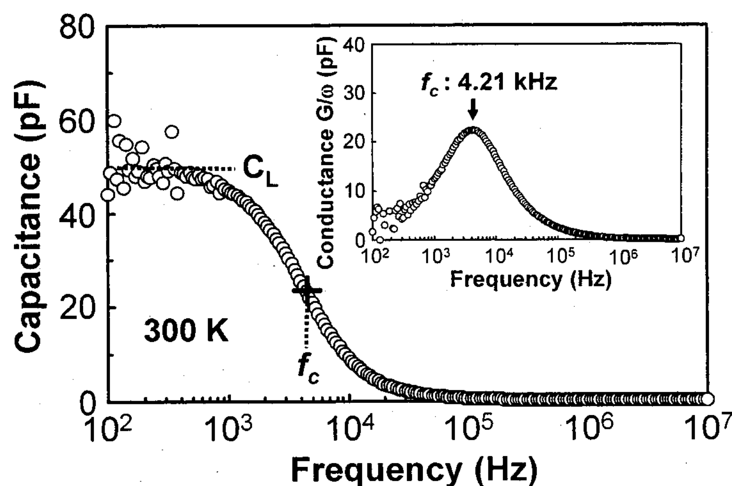

FIG. 4.2. Room-temperature frequency dependence of capacitance for Be-implanted GaN after annealing at 1050 °C. The inset shows the frequency dependence of conductance at room temperature.

determined by the carrier exchange between the Be-related impurity level and the valence band, reflecting the electrical activity of the implanted Be atoms, whereas above the capacitance cutoff frequency f_c (impurity transition frequency), the hole modulation of the depletion layer edge governs the electrical response. Considering that the conductance G/ω presents a peak at the f_c, the characteristic frequency f_c is estimated to be ~4.2 kHz, as shown in the inset of Fig. 4.2. From these C-f and G/ω-f data, meaningful C-V measurements need to be performed at frequencies lower than the f_c.

Figure 4.3 shows room-temperature $1/C^2$-V plots at a frequency of 1 kHz for a Schottky diode fabricated on the Be-implanted GaN. From the slope of these plots, the effective acceptor concentration is estimated to be ~1.2×10^{17} cm^{-3}, which seems to be distributed almost uniformly over the depth of the capacitance measurement. Here, this value obtained at 1 kHz implies the net acceptor concentration (N_a - N_d) rather than the hole concentration. This effective acceptor concentration is much smaller than the Be concentration determined by the SIMS measurements. This indicates that the implanted Be atoms are slightly activated by annealing at 1050 °C. By extrapolating the line fitted to the $1/C^2$-V plots to the voltage axis as shown in Fig. 4.3, the barrier height ϕ_b of the fabricated Pt-Schottky diode is estimated to be ~1.4 eV.

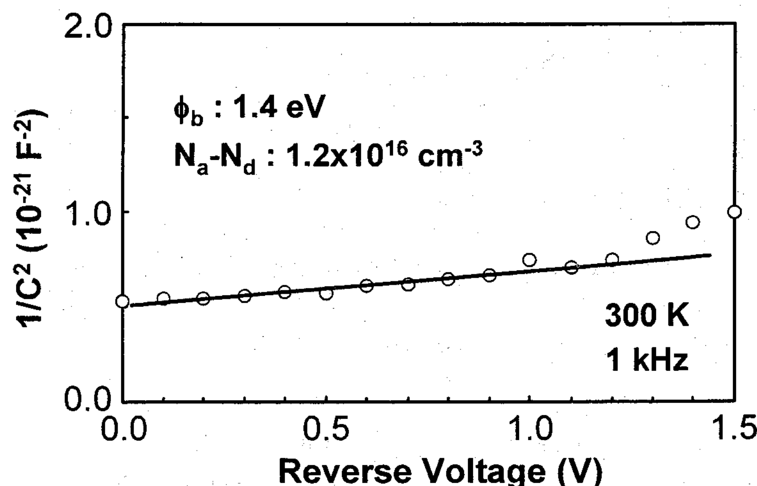

FIG. 4.3. Room-temperature capacitance-voltage characteristics at a frequency of 1 kHz for Be-implanted GaN after annealing at 1050 °C.

Figure 4.4 shows typical TAS spectra measured for the Schottky diode fabricated on Be-implanted GaN under zero dc bias. A dominant peak can be clearly seen in the spectra. This peak shifts to higher temperatures with increasing measurement frequency. Thus, this peak is assigned to a deep level. By contrast, no TAS peaks could be detected in the N-implanted GaN sample. This result implies that the deep level observed in the Be-implanted sample is not related to implantation-induced defects, because N implantation should introduce at least as much damage into the GaN as Be implantation due to its heavier ion mass. Additionally, the damage introduced by N implantation has also previously been reported in the literature to be entirely restored by high-temperature annealing [19,20]. Therefore, this deep level detected in the Be-implanted GaN is considered to be associated with the Be doping. Arrhenius analysis for the hole emission rate e_p/T^2 of the corresponding level yields an activation energy of ~231 meV for hole emission into the valence band, as shown in the inset of Fig. 4.4. Here, the data was analyzed under the assumption of a

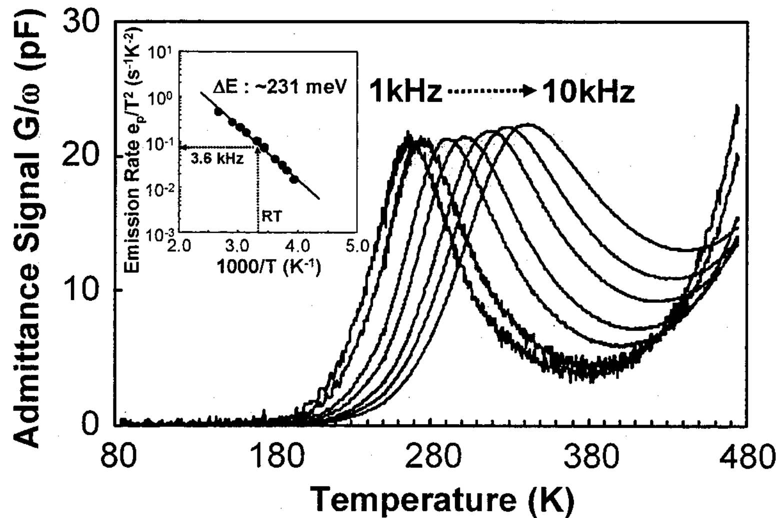

FIG. 4.4. TAS spectra at various frequencies between 1 - 10 kHz for Be-implanted GaN after annealing at 1050 °C. The inset shows Arrhenius plots of the hole emission rate, e_p/T^2.

temperature-independent cross-section. The characteristic frequency corresponding to this energy level at room temperature (300 K) is calculated to be ~3.6 kHz, which can be extracted from a line fitted to the Arrhenius plots, as shown in the inset of Fig. 4.4. This frequency is found to be in reasonable agreement with the f_c of ~4.2 kHz estimated from the room temperature *C-f* and *G/ω-f* curves in Fig. 4.2. Therefore, this energy level should be assigned to the Be-related acceptor level. In addition, it makes no sense to suggest that hydrogen penetrates the thick encapsulation cap during annealing. Thus, this energy level is probably associated with isolated Be atoms rather than Be-H complexes.

This acceptor level that we have obtained seems to be in agreement with the value of 250 meV reported by Salvador *et al.* [13], but it is apparently much deeper than the theoretically expected value of ~60 meV when Be atoms only reside at Ga-lattice sites in GaN [10]. Thus, this deepening of the activation energy for the Be acceptor may be associated with imperfect incorporation of the implanted Be atoms, which results in the slight electrical activation, as stated above. Therefore, some co-implantation technique based on a site-competition effect may be effective in enhancing the electrical activation of the implanted Be atoms [8,17,19,21].

In order to increase the probability of the implanted Be atoms occupying a Ga-lattice site, Be+N co-implantation into undoped GaN was also carried out. The N/Be ratio dependence of the Be acceptors was investigated in the Be+N co-implantation process. Figure 4.5 shows a typical series of TAS spectra for the Schottky diodes fabricated on Be+N co-implanted GaN with various N/Be ratios under zero dc bias. With an introduction of additional N atoms, the Be acceptor concentration is found to decrease significantly in addition to an increase in the thermal activation energy for the Be acceptors. This result probably indicates the formation of some Be-N compounds (Be_3N_2) during activation annealing process, resulting in the decrease in effective Be acceptor concentration. Conversely, we can say that implanted Be atoms are easily combined with the component N atoms of GaN and that possible Be dopant atoms decreases subsequently. As a result, the Be activation efficiency substantially becomes poor by using any Be implantation techniques.

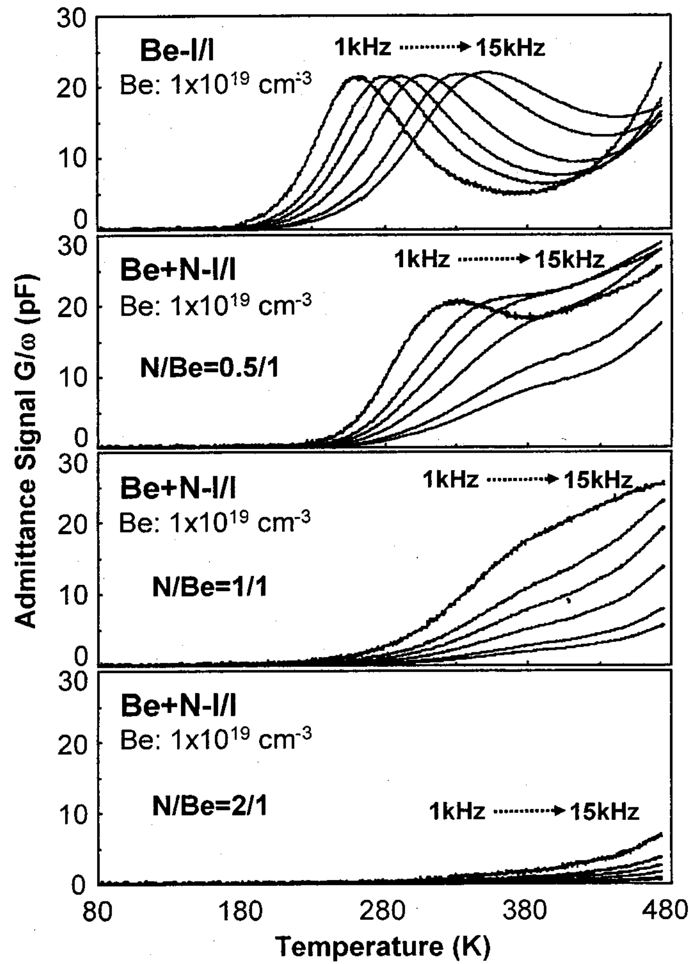

FIG. 4.5. N/Be ratio dependence of TAS spectra at various frequencies between 1 and 15 kHz for Be+N co-implanted GaN after annealing at 1050 °C.

In summary, the acceptor levels of Be-implanted and subsequently annealed GaN have been investigated electrically. TAS measurements revealed a dominant deep level with an activation energy of ~231 meV from the valence band, which is in reasonable agreement with the frequency dependence of capacitance and conductance in view of the impurity transition frequency at room temperature. Therefore, this energy level is most probably associated with a Be-related deep acceptor.

4.3 Be+O Co-Implantation

4.3.1 Experimental

The epitaxial GaN films used in these experiments were 2.5 μm thick. They were grown on a-plane sapphire substrates by atmospheric pressure MOCVD at 1130 °C, with a pre-deposited 20 nm AlN buffer layer grown at 420 °C. The GaN films were not intentionally doped, but had a background n-type carrier concentration of ~$5x10^{15}$ cm^{-3}. After growth, the GaN samples were implanted, using O_2 gas and Be metal as the sources of the $^{16}O^+$ and $^9Be^+$ species, respectively. Prior to the O^+ implantation, a 100-nm-thick Ni layer was deposited on the top surface of the samples by electron-beam evaporation in order to reduce the implantation-induced damage. Then, multiple step O^+ implantation was performed as follows. The O^+ ions were implanted at 400, 300, 250, 200, 150, and 110 keV with dosages of $4.5x10^{14}$, $8x10^{13}$, $1.2x10^{14}$, $1.3x10^{14}$, $7x10^{13}$, and $1.5x10^{14}$ cm^{-2}, respectively, to produce a mean O concentration of $2x10^{19}$ cm^{-3} to a depth of ~0.4 μm. After removing the Ni layer, a 300-nm-thick Ni layer was deposited again prior to the Be^+ implantation. Then, multiple step Be^+ implantation was performed; the Be^+ ions were implanted at 350, 250, and 170 keV with dosages of $6x10^{14}$, $2.5x10^{14}$, and $4x10^{14}$ cm^{-2}, respectively, to produce a mean Be concentration of $2x10^{19}$ cm^{-3} to a depth of ~0.4 μm. Conventional Be- and O-implanted GaN samples were also prepared with mean concentrations of $2x10^{19}$ cm^{-3} (depth = 0.4 μm) for reference. In the case of the Be+O co-implantation, the O/Be ratio was kept at 1 for optimum doping [17,19,21]. All of the implants were carried out at room temperature, with an incident angle 7° off the surface normal. After implantation, the Ni layer was removed and then a 500-nm-thick SiO_2 capping layer was deposited on the surface by radio-frequency sputtering at room temperature to provide an encapsulation cap for the subsequent implant activation anneal. All of the samples were annealed at temperatures between 950 and 1100 °C for 5 min in flowing N_2 gas. Following the annealing step, HF was used to remove the SiO_2 cap. The carrier type of the Be- and Be+O-implanted GaN samples was determined by room-temperature Hall-effect and electrical measurements. For the conventional O-implanted samples, the implanted O atoms became electrically active as an n-type dopant after annealing at 1100 °C, as reported in section 2.4. Some electrical

measurements were conducted on lateral dot-and-ring Schottky diodes fabricated using Pt as a Schottky metal [15,18,22,23]. Capacitance-frequency (C-f), conductance-frequency (G/ω-f), and capacitance-voltage (C-V) measurements were performed at room temperature with an ac modulation level of 30 mV and frequencies ranging from 100 Hz to 10 MHz. TAS measurements were performed at an ac modulation level of 30 mV and frequencies ranging from 100 Hz to 30 kHz, covering the temperature range from 85 to 480 K. The depth distribution of the implanted O and Si atoms was measured by SIMS. The surface morphology of the implanted region of the GaN samples was analyzed by atomic force microscopy (AFM).

4.3.2 Results and Discussion

Figure 4.6 shows typical SIMS profiles of the implanted O and Be atoms both before and after annealing at 1050 °C, together with O and Be atomic profiles calculated by TRIM. The Be concentration to a depth of ~0.4 μm is confirmed to be about $2\text{x}10^{19}$ cm^{-3} for both Be- and Be+O-implanted GaN samples before the activation anneal, which is in reasonable agreement with a calculation made using a TRIM code. Additionally, annealing causes the implanted Be atoms to diffuse slightly towards the near-surface region (~100 nm from the surface) regardless of the implantation of additional O atoms. The Be-diffusion level is almost the same under all annealing conditions, resulting in identical Be SIMS profiles regardless of the annealing temperature. Moreover, SIMS profiles of implanted O atoms both before and after annealing are unchanged, in agreement with the profiles calculated by TRIM. Furthermore, no Ni atoms are detected for all of the implanted samples. This suggests that the diffusion of Ni atoms into GaN from the Ni layer does not occur during the implantation process and consequently that the use of the Ni layer for reducing the implantation-induced damage does not influence the Be-doping characteristics, as discussed later.

Figure 4.7 shows the room-temperature sheet carrier concentration, n_s, of the Be- and Be+O-implanted GaN samples as a function of annealing temperature. The behavior of n_s may be classified into three regions (a), (b), and (c) in view of the carrier type. In region (b) where the annealing temperature is between 1000 and 1050 °C, the n_s tends to decrease significantly for both Be- and Be+O-implanted samples. These

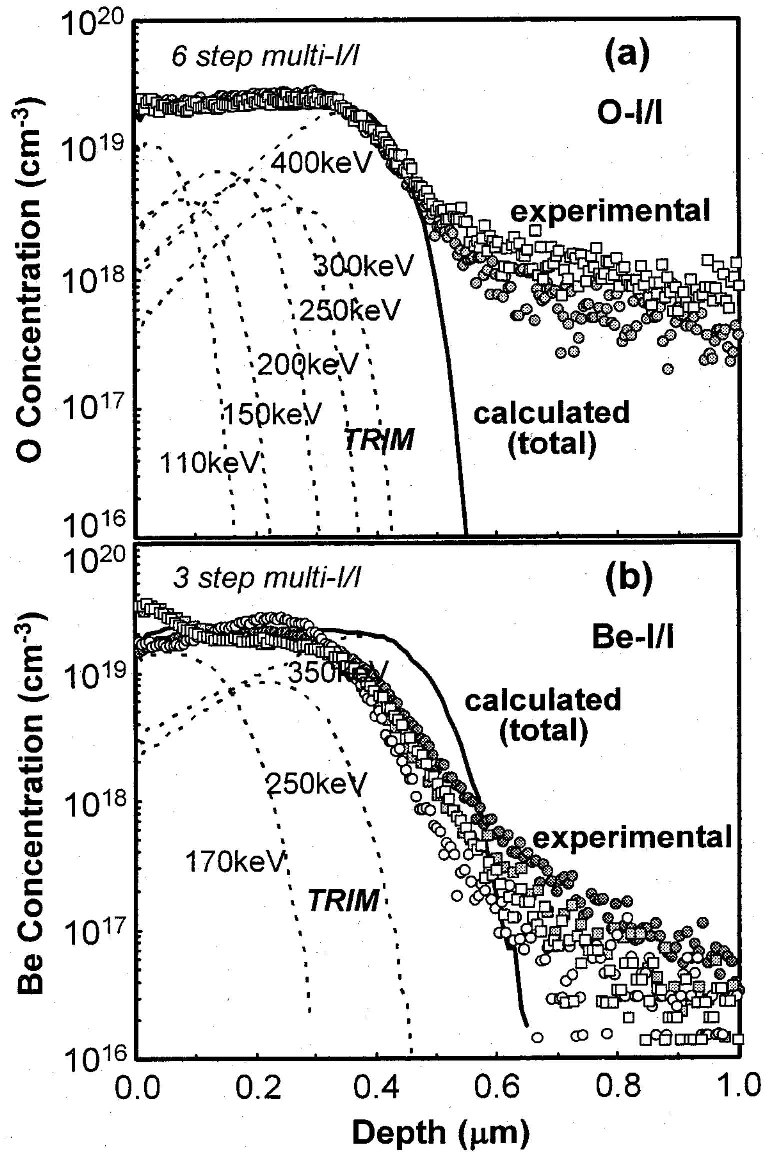

FIG. 4.6. TRIM simulated atomic profiles of implanted (a) O and (b) Be atoms and SIMS profiles of (a) O and (b) Be in Be- and Be+O-implanted GaN, as implanted (○, ●) and annealed (■, □) at 1050 °C, respectively.

samples are the only ones displaying p-type characteristics, with small mobility, μ, in the region of 1 - 3 cm^2/Vs. Furthermore, the n_s of the Be+O-implanted samples is relatively higher than that of the Be-implanted samples, indicating that the implantation of additional O atoms improves the electrical p-type

activation. On the other hand, samples annealed in regions (a) and (c) show n-type characteristics, which may be caused by the implantation-induced damage and the formation of N vacancies during the anneal, respectively. In particular, the significant increase in n_s seen for the Be+O-implanted sample after annealing at 1100 °C is considered to be due to the combined effect of N-vacancy formation and electrical O-activation induced by high-temperature annealing, as stated above [24].

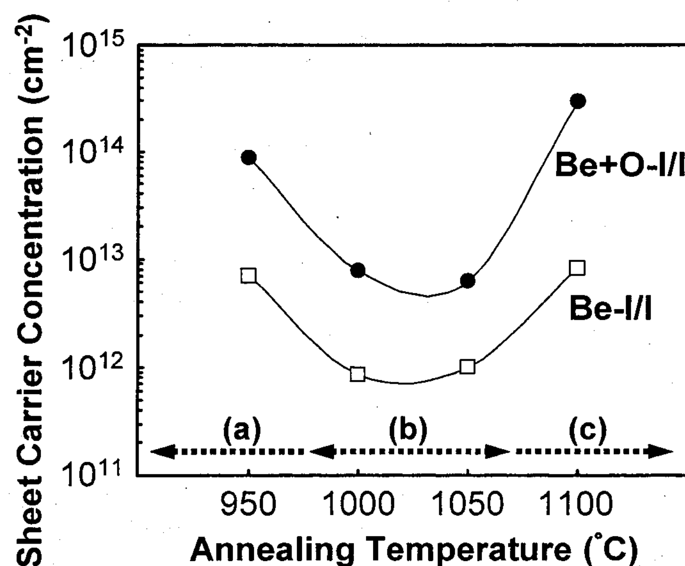

FIG 4.7. Sheet carrier concentration as a function of annealing temperature for Be- and Be+O-implanted GaN.

Figure 4.8 shows room-temperature *C-f* curves at zero dc bias for Schottky diodes based on Be- and Be+O-implanted GaN samples after annealing at 1050 °C. Regardless of the O-implantation, the measured capacitance varies markedly with frequency for both samples. This variation in capacitance is most likely due to a typical dispersion effect characteristic of deep Be acceptors; depending on frequency, there is competition between deep impurities and the dopant character [6,7]. Here, the low-frequency capacitance C_L is determined by carrier exchange between the Be-related impurity level and the valence band, reflecting

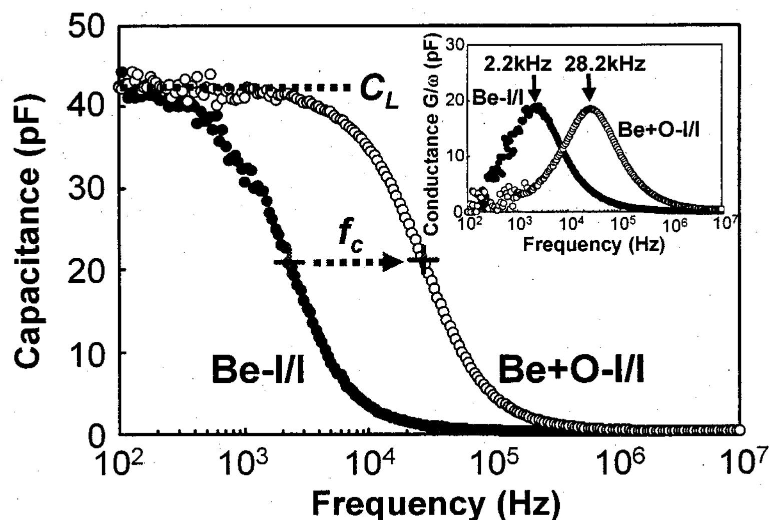

FIG. 4.8. Room-temperature frequency dependence of capacitance for Be- and Be+O-implanted GaN after annealing at 1050 °C. The inset shows the frequency dependence of conductance at room temperature.

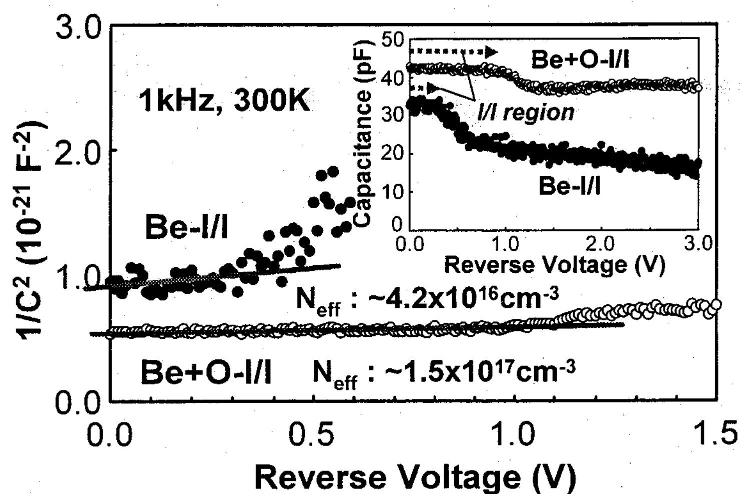

FIG. 4.9. Room-temperature $1/C^2$-V plots at a frequency of 1 kHz for Be- and Be+O-implanted GaN after annealing at 1050 °C. The inset shows room-temperature C-V curves at 1 kHz.

the electrical activity of the implanted Be atoms, whereas above the capacitance cutoff frequency f_c (impurity transition frequency), the hole modulation of the depletion layer edge governs the electrical response. In view of the fact that there is a peak at f_c in the conductance G/ω, the characteristic frequencies f_c are estimated to be ~2.2 and ~28.2 kHz for the Be- and Be+O-implanted samples, respectively, as shown in the inset of Fig. 4.8. Thus, a significant increase in f_c occurs due to the implantation of additional O atoms. This result indicates that shallower acceptor levels may be newly formed by co-implantation of Be^+ and O^+ based on a site-competition effect [17,18]. From C-V measurements at 1 kHz (Fig. 4.9), the net acceptor concentration (N_a - N_d) was calculated to be ~1.5×10^{17} cm^{-3} for the Be+O-implanted sample. As shown in Fig. 4.8, C_L is estimated to be about 43 pF for both samples, which suggests that the effective acceptor concentration of the Be-implanted sample is at the same level as that of Be+O-implanted sample. These acceptor concentrations are much smaller than the Be concentration of 2×10^{19} cm^{-3} determined by the SIMS measurements. This result indicates that much implantation-induced damage still remains and may compensate for the holes generated by the deep Be acceptors in both samples. Therefore, the higher Be activation rate caused by the introduction of O atoms is most likely to dominate the improvement of the p-type doping characteristics, as stated in Fig. 4.7.

Figures 4.10 (a) and 4.10 (b), respectively, show typical TAS spectra measured under zero dc bias for Schottky diodes fabricated on Be- and Be+O-implanted GaN and annealed at 1050 °C. Depending on the implant conditions, the TAS spectra reveal two kinds of peak denoted by A_1 and A_2. These peaks shift towards higher temperatures with an increasing hole emission rate, which can be calculated from the measurement frequency. This implies that these peaks are associated with Be-related deep acceptor levels [15], as discussed in section 4.2. As shown in Fig. 4.11, the thermal activation energy for hole emission into the valence band is estimated from Arrhenius plots of the hole emission rate e_p/T^2 for the corresponding level in the both spectra. Here, the data are analyzed under the assumption that the cross-section is temperature-independent. For the conventional Be-implanted sample, a dominant peak A_1 is clearly observed, corresponding to a Be-related acceptor level with a thermal activation energy of ~240 meV. This

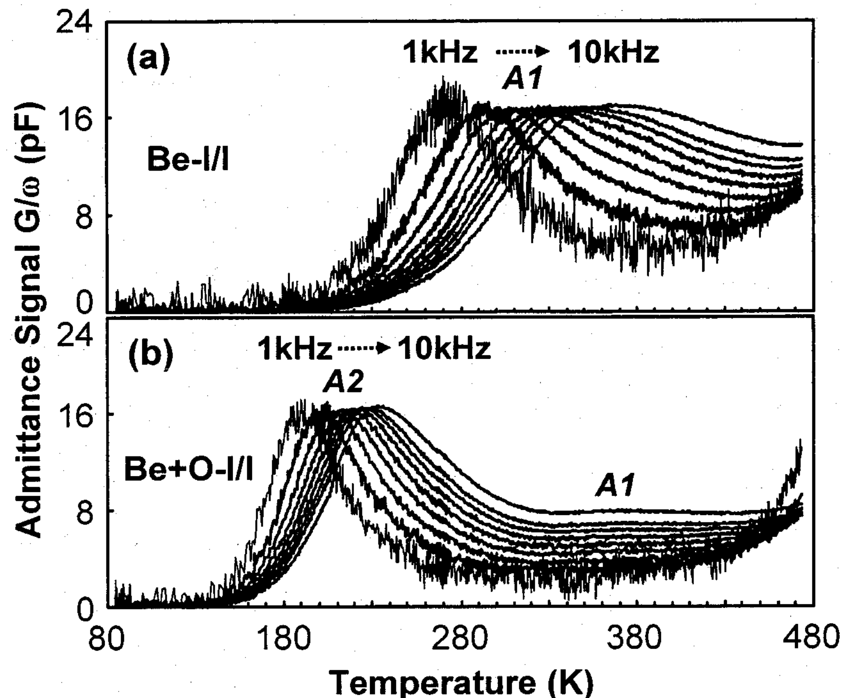

FIG. 4.10. TAS spectra at various frequencies between 1 and 10 kHz for (a) Be- and (b) Be+O-implanted GaN after annealing at 1050 °C.

value is very close to the previously reported one [15]. For the Be+O-implanted sample, a dominant peak A_2 is seen in addition to the peak A_1. This newly observed A_2 peak is located at ~163 meV above the valence band. Thus, the Be-related acceptor level is found to decrease significantly with the introduction of O atoms. This behavior of the acceptor level, i.e., becoming shallower, seems to be in good agreement with the increase in impurity transition frequency f_c by implantation of additional O atoms (Fig. 4.8). The characteristic frequencies corresponding to the A_1 and A_2 peaks at room temperature (300 K) are calculated to be ~1.3 and ~43.1 kHz, which can be extracted from the Arrhenius plots, as shown in Fig. 4.11. These values are in reasonable agreement with the values of f_c of ~2.2 and ~28.2 kHz estimated from the

room-temperature C-f and G/ω-f curves in Fig. 4.8. Therefore, this confirms that these acceptor levels are attributable to the implanted Be atoms. Bearing in mind the site-competition effect caused by the implantation of additional O atoms, the A_1 and A_2 levels can probably be assigned to Be atoms occupying interstitial and Ga-lattice sites, respectively. Therefore, the decrease in the Be-related acceptor level with the introduction of O atoms is most likely to enhance the Be activation rate, which results in an improvement of the p-type doping characteristics, as stated above. In addition, a significant reduction in residual n-type carriers that act in competition with the p-type carriers is required in order to realize increasing p-type doping characteristics.

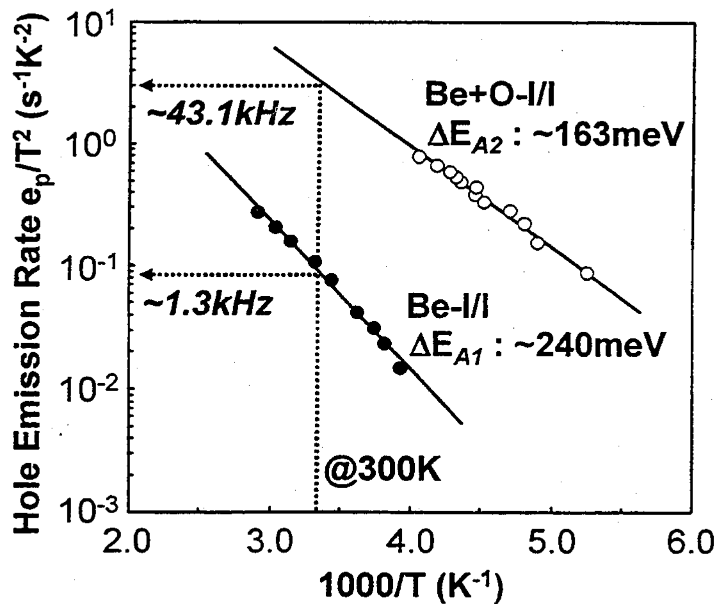

FIG 4.11. Arrhenius plots of the hole emission rate e_p/T^2 for Be- and Be+O-implanted GaN after annealing at 1050 °C.

Figures 4.12 (a) and 4.12 (b), respectively, show typical AFM images of the Be- and Be+O-implanted GaN samples after annealing at 1050 °C. Smooth surface morphology with mean roughness R_{ms} of ~0.62

nm can be obtained in both samples even after the activation annealing process. Additionally, in both samples, a number of growth steps are clearly observed, which surface morphology is almost identical with that of the as-grown GaN before implantation. In other words, the surface morphology is found to be unchanged even after the implantation and subsequent annealing processes for both implanted GaN samples. However, implantation-induced micro-defects "small holes" can be seen even after the high-temperature annealing process for both Be- and Be+O-implanted samples, which is the same behavior as that of Si- and Si+N-implanted GaN after activation annealing process, as reported in section 2.3. Thus, the micro-defects observed in both the Be- and Be+O-implanted GaN are probably associated with the implantation of Be atoms. The micro-defect density observed in the Be+O co-implanted GaN seems to be a little more than that in the Be-implanted GaN. In addition, the micro-defects are thought to correspond to the dislocations, where some parts of the implanted Be atoms may be captured, resulting in the significant decrease in effective acceptor concentration, as stated above.

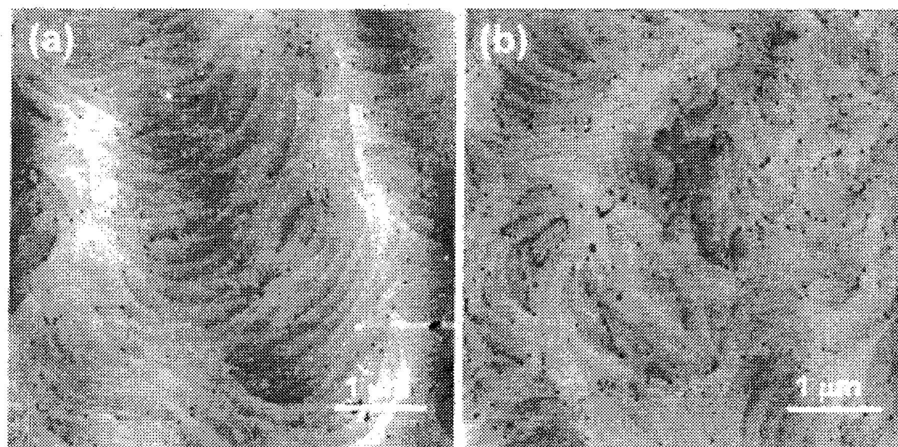

FIG. 4.12. AFM images of (a) Be- and (b) Be+O-implanted GaN samples with a mean Be concentration of $2x10^{19}$ cm^{-3} (a depth of ~0.4 μm) after annealing at 1050 °C. Both images are 5x5 μm^2.

In summary, we have electrically investigated the effect of Be+O co-implantation on Be acceptors in GaN. From TAS and *C-f* measurements, the implantation of additional O^+ ions is found to decrease the Be-related acceptor level from ~240 to ~163 meV due to a site-competition effect. This behavior of the acceptors is in reasonable agreement with the improvement of p-type doping characteristics as determined by room-temperature Hall-effect measurements. Therefore, this acceptor level can probably be assigned to Be atoms residing on interstitial and Ga-lattice sites in GaN.

4.4 Conclusion

P-type regions were produced in undoped GaN films by Be^+ and Be^++O^+ implantation and subsequent annealing at temperatures between 1000 and 1050 °C. From TAS measurements, the activation energy of the Be acceptor level was found to decrease from ~240 to ~163 meV by the implantation of additional O atoms, which is in reasonable agreement with the improvement in p-type doping characteristics determined by room-temperature Hall-effect measurements. These results indicate that the Be^++O^+ co-implantation reduces the depth of the Be acceptor level based on a site-competition effect. Therefore, these acceptor levels are most probably attributable to Be atoms at interstitial and Ga-lattice sites.

References

[1] M. A. Khan, A. R. Bhattarai, J. N. Kuznia, and D. T. Olson, Appl. Phys. Lett. 63, 1214 (1993).

[2] J. C. Zolper, R. J. Shul, A. G Baca, R. G Wilson, S. J. Pearton, and R. A. Stall, Appl. Phys. Lett. **68**, 2273 (1996).

[3] A. P. Zhang, J. W. Johnson, F. Ren, J. Han, A. Y. Polyakov, N. B. Smirnov, A. V. Govorkov, J. M. Redwing, K. P. Lee, and S. J. Pearton, Appl. Phys. Lett. **78**, 823 (2001).

[4] T. Tanaka, A. Watanabe, H. Amano, Y. Kobayashi, K. I. Akasaki, S. Yamazaki, and M. Koide, Appl. Phys. Lett. **65**, 593 (1994).

[5] C. Johnson, J. Y. Lin, H. X. Jiang, M. A. Khan, and C. J. Sun, Appl. Phys. Lett. **68**, 667 (1996).

[6] J. W. Huang, T. F. Kuech, H. Lu, and I. Bhat, Appl. Phys. Lett. **68**, 2392 (1996).

[7] D. Seghier and H. P. Gislason, Appl. Phys. Lett. **88**, 6483 (2000).

[8] D. G. Kent, M. E. Overberg, and S. J. Pearton, J. Appl. Phys. **90**, 3750 (2002).

[9] Y. Nakano, T. Kachi, and T. Jimbo, (unpublished).

[10] F. Bernardini, V. Fiorentini, and A. Bosin, Appl. Phys. Lett. **70**, 2990 (1997).

[11] J. Neugebauer and C. G. Van de Walle, J. Appl. Phys. **85**, 3003 (1999).

[12] O. Brandt, H. Yang, H. Kostial, and K. H. Ploog, Appl. Phys. Lett. **69**, 2707 (1996).

[13] A. Salvador, W. Kim, Ö. Aktas, A. Botchkarev, Z. Fan, and H. Morkoç, Appl. Phys. Lett. **69**, 2692 (1996).

[14] C. Ronning, E. P. Carlson, D. B. Thomson, and R. F. Davis, Appl. Phys. Lett. **73**, 1622 (1998).

[15] Y. Nakano and T. Jimbo, Appl. Phys. Lett. **81**, 3990 (2002).

[16] H. Kobayashi and W. H. Gibson, Appl. Phys. Lett. **74**, 2355 (1999).

[17] Y. Nakano, R. K. Malhan, T. Kachi, and H. Tadano, J. Appl. Phys. **89**, 5961 (2001).

[18] Y. Nakano, T. Kachi, and T. Jimbo, Appl. Phys. Lett. **82**, 2082 (2003).

[19] Y. Nakano, T. Kachi, and T. Jimbo, Jpn. J. Appl. Phys. **41**, 2522 (2002).

[20] D. Haase, M. Schmid, W. Kürner, A. Dörnen, V. Härle, F. Scholz, M. Burkard, and H. Schweizer, Appl. Phys. Lett. **69**, 2525 (1996).

[21] Y. Nakano and T. Jimbo, J. Appl. Phys. **92**, 3815 (2002).

[22] Y. Nakano and T. Kachi, Appl. Phys. Lett. **79**, 1631 (2001).

[23] Y. Nakano and T. Jimbo, J. Appl. Phys. **92**, 5587 (2002).

[24] Y. Nakano, T. Kachi, and T. Jimbo, J. Vac. Sci. Technol. B (in press).